A Novel CNN-Based Radar Reflectivity Retrieval Network Using Geostationary Satellite Observations

Jianwei Si, Xingwang Li, Haonan Chen, *Senior Member, IEEE*, and Lei Han, *Member, IEEE*

***Abstract*— A ground-based weather radar is commonly used for observing severe convective weather. However, the limited coverage of the radar poses difficulties in obtaining reliable radar observations for oceanic and mountainous regions. An effective solution is to derive radar data from meteorological satellite observations using deep-learning methods. This study proposes a novel feature redistribution module-based convolutional neural network (FR-CNN) to retrieve radar composite reflectivity (CREF) data from geostationary satellite observations. Differing from existing skip connection (SC)-based CNNs, FR-CNN adopts a feature redistribution module (FRM) to alleviate the problem of information scarcity during network propagation. In the FRM, a parallel attention block (PAB) is introduced to preserve key feature information and improve the retrieval ability of the FR-CNN. The evaluation results show that the FR-CNN can effectively reconstruct radar reflectivity data and has a better performance than other methods like U-Net in terms of assessment indices including the probability of detection (POD), false alarm ratio (FAR), and critical success index (CSI).**

***Index Terms*— Convolutional neural networks (CNNs), deep learning, geostationary satellite, weather radar.**

I. Introduction

SEVERE convective weather events such as extreme precipitation pose a significant threat to human safety, leading to potential damages and mortality [1]. The ground-based weather radar is regarded as the primary observation instrument for monitoring convective events, providing high resolution and reliable information for accurate extreme weather forecasting [2], [3], [4]. However, the inherent limitations of the ground-based weather radar, such as complex terrains and high deployment costs, impose significant constraints on radar coverage in specific regions, particularly mountainous and oceanic areas.

Compared with the ground-based radar, geostationary meteorological satellites can offer prominent advantages in terms of continuous and wide-ranging observations with high spatial and temporal resolutions, which enables the timely tracking of convective events in specific regions [5], [6], [7]. As satellites can observe clouds that cannot be seen by the radar due to terrain occlusion, using satellite observations to reconstruct radar data is a valuable endeavor, especially in the regions without radar coverage, which can effectively enhance the forecasting capability for severe convective weather events within these areas [8].

Recently, deep-learning technology has made remarkable strides in various scientific fields. Convolutional neural networks (CNNs), in particular, have been widely applied in diverse domains, including object detection, semantic segmentation, target tracking, as well as the remote-sensing field [9], [10], [11]. Hilburn et al. [12] proposed a U-Net method to derive radar reflectivity from satellite observations and lightning data. Duan et al. [8] extended the above U-Net method to another geostationary satellite (i.e., Himawari-8). The input of the network is the brightness temperature (BT) data of five infrared channels of Himawari-8. The output is the composite reflectivity (CREF, the maximum base reflectivity factor). Similar to [8], Sun et al. [13] utilized BT data from the Fengyun-4A (FY-4A) meteorological satellite along with the U-Net to reconstruct radar reflectivity in the regions lacking radar coverage. In addition, Yang et al. [14] introduced an attention mechanism-based U-Net to reconstruct radar reflectivity using FY-4A observations, yielding improved retrieval results. The retrieval networks mentioned above incorporate skip connections (SCs) to mitigate the loss of feature information caused by downsampling operations.

In this study, we propose a novel CNN-based radar reflectivity retrieval network based on the feature redistribution module-based CNN (FR-CNN) to retrieve CREF radar observations using satellite data. Compared with conventional U-Net, the FR-CNN adopts a feature redistribution module (FRM) to replace the SC operation. The FRM is designed to incorporate a parallel attention block (PAB) to preserve key spatial and channel information simultaneously, thus more inner structure of radar echoes can be captured. The rest of this letter is organized as follows. Section II introduces the data used in this study. Section III presents the architecture and details of the proposed FR-CNN. We evaluate the performance of the FR-CNN and other methods in Section IV. Finally, the conclusion is depicted in Section V.

II. Data

The BT data and the CREF data are used in this study. All of the data are collected by the China Meteorological Administration (CMA). Fig. 1 shows our study domains including

Manuscript received 6 August 2023; revised 30 October 2023; accepted 9 November 2023. Date of publication 15 November 2023; date of current version 19 December 2023. This work was supported by the National Natural Science Foundation of China under Grant 42275003. The work of Haonan Chen was supported by Colorado State University. *(Jianwei Si and Xingwang Li are co-first authors.) (Corresponding author: Lei Han.)*

Jianwei Si, Xingwang Li, and Lei Han are with the Faculty of Information Science and Technology, Ocean University of China, Qingdao 266404, China (e-mail: sjw9002@stu.ouc.edu.cn; lixingwang@stu.ouc.edu.cn; hanlei@ouc.edu.cn).

Haonan Chen is with the Department of Electrical and Computer Engineering, Colorado State University, Fort Collins, CO 80523 USA (e-mail: haonan.chen@colostate.edu).

Digital Object Identifier 10.1109/LGRS.2023.3332844

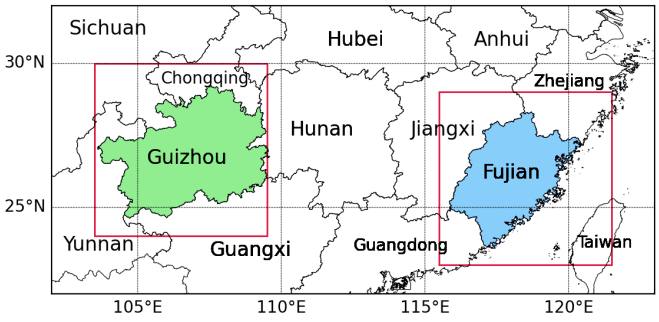

Fig. 1. Demonstration of study domains (red rectangles).

Fujian province (marked as FJ), encompassing a latitude range of 23°N–29°N and a longitude range of 115.5°E–121.5°E, and Guizhou province (marked as GZ), covering a latitude range of 24°N–30°N and a longitude range of 103°E–109°E. The proposed deep-learning model (FR-CNN) is trained and tested over FJ. Then, the model is used over GZ to assess its generalization and practical application capability.

The BT data of Chinese regions are provided by the advanced geosynchronous radiation imager (AGRI) carried on the Fengyun-4A satellite with temporal and spatial resolutions of 5 min and 4 km, respectively. Inspired by [13] and [14], three channel observations at wavelengths of 3.75, 6.90, and 10.70 μm are used in this study. For the retrieved CREF, it has the same temporal resolution as the satellite data. In this study, the time interval of retrieved CREF is also 5 min.

Considering the differences in spatiotemporal resolution of satellite and radar observations, we apply a bilinear interpolation approach [15] to adjust the satellite data resolution to 1 km to ensure consistency in spatial resolution. Finally, we collected 17 476 samples from May to June 2019, where 13 980 samples were collected from May to July for training and validation (80% of the data) and 3496 samples collected in August for testing (20% of the data) over the FJ area. For the generalization test purpose, we used 3936 samples collected from May 1 to May 31, 2019, over the GZ area.

III. Methodology

Fig. 2 presents an overview of the workflow of the FR-CNN. The proposed model is mainly composed of three components including an encoder, an FRM, and a decoder. The inputs of the model are BT data, and the outputs are CREF reconstructions. More details are given in Sections III-A–III-C.

A. Encoder

The structure of the encoder can be found in Fig. 2, which consists of one convolution module (marked as CM-1) and three pooling modules (marked as PM-1, PM-2, and PM-3). The input of the encoder is multiband satellite data.

The input data are followed by a series of modules including CM-1, PM-1, PM-2, and PM-3. The structure of CM-1 can be found in Fig. 3(a). The module consists of two convolutional layers. Each layer includes a convolution operation followed by rectified linear units (ReLUs) [10]. The size and number of convolution kernels in the layers are set to 3 × 3 and 256, respectively.

Following CM-1, three pooling modules, namely PM-1, PM-2, and PM-3, are designed. The structure of these modules is illustrated in Fig. 3(b). Similar to the CM module, these modules also consist of two convolutional layers. However, a max-pooling operation is utilized to reduce the dimension of feature maps. In this study, the pooling stride is assigned to 2, and the size of the convolution kernels in PM-1, PM-2, and PM-3 is set to 3 × 3. The number of convolution kernels in the modules is assigned to 32, 64, and 128, respectively. The ReLU activation function is employed in all layers.

B. Feature Redistribution Module

For conventional U-Net, the SC is adopted to suppress the loss of pristine information during network propagation. However, for the feature maps of the connections, pristine information is not fully included, which may result in less details of strong echoes. Therefore, inspired by [16] and [17], to capture more details of the inner structure of strong echoes, an attention-based FRM is designed. The module adopts a residual block (RB) to extract features of input connections. A PAB (i.e., PAB) is then employed to reserve key spatial and channel information simultaneously, which can enable the FRM to capture more inner structure of radar echoes. Due to sufficient consideration of pristine information and attention mechanism, the module can effectively mitigate the issue of information shortage of SC during network propagation.

The proposed FRM regards the output feature maps of CM-1, PM-1, and PM-2 as inputs. Since these PM modules have different sizes compared to the CM module, we upsample them using transpose convolution operations to ensure consistency in size. The strides of the transpose convolution operations in the modules are set to 1, 2, and 4, respectively. Subsequently, we concatenate the processed feature maps for further operations.

Following the concatenation step, the obtained feature map is fed into an RB to extract complex characteristics. The architecture of the residual module is depicted in Fig. 3(c). The RB consists of several operations, including convolution, batch normalization (BN), and ReLU activation function. Notably, to prevent information loss during these operations, the input feature map is element-wise added to the map obtained after the second BN operation. Finally, the ReLU activation function is applied to obtain the output of the RB. The kernel size of the convolution operations is set to 3 × 3, and the number of convolution kernels is set to 224 for both operations within the RB.

To preserve key feature information of RB, we introduce a PAB. The structure of PAB is illustrated in Fig. 4. The block consists of three branches: spatial branch, channel branch, and input branch. Let X represent the input of PAB, which is also the output of the RB. The output of the spatial branch can be obtained as follows:

$$W_{\text{spatial}} = \sigma(\text{conv}(\text{concat}(\text{AP}(X), \text{MP}(X)))) \quad (1)$$

where $\sigma(\cdot)$, conv$(\cdot)$, concat$(\cdot)$, AP$(\cdot)$, and MP$(\cdot)$ represent the operations including sigmoid, convolution, concatenation,

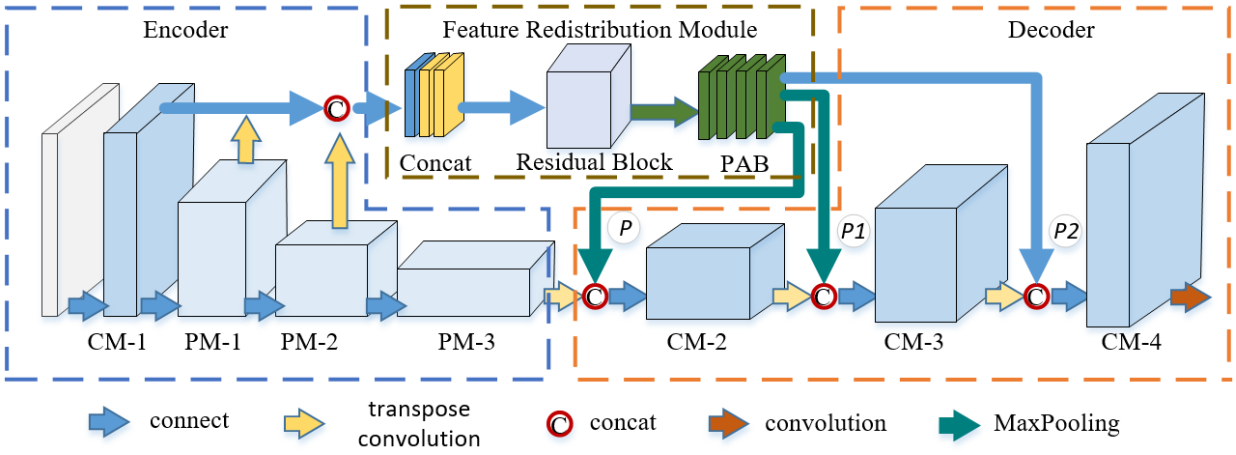

Fig. 2. Architecture of the proposed FR-CNN.

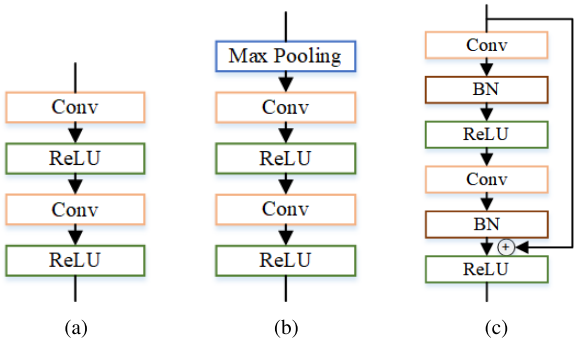

Fig. 3. Structure of CM, PM, and RB. (a) CM. (b) PM. (c) RB.

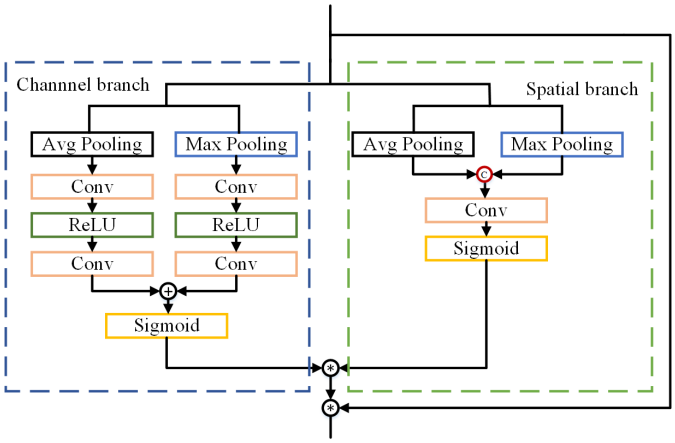

Fig. 4. Flowchart of PAB.

average-pooling, and max-pooling, respectively. In this study, the kernel size of convolution operations is assigned to 7×7. The number of convolution kernels is set to 1. Similarly, the output of the channel branch can be acquired as follows:

$$W_{\text{channel}} = \sigma(\lambda_1 \times \text{conv}(\text{ReLU}(\text{conv}(\text{AP}(X)))) + \lambda_2 \times \text{conv}(\text{ReLU}(\text{conv}(\text{MP}(X))))) \quad (2)$$

where λ_1 and λ_2 are the weight parameters that are set to $\lambda_1 = \lambda_2 = 0.5$ after tuning them from {(0.4, 0.6), (0.5, 0.5), (0.6, 0.4), (1, 1)}. The kernel size of both convolution operations is set to 3×3 [16]. The number of convolution kernels is assigned to 224. The attention weights can be obtained from various branches of PAB as follows:

$$W_{\text{attention}} = W_{\text{spatial}} * W_{\text{channel}} * X \quad (3)$$

where $*$ denotes the Hadamard product [18]. Through PAB, the feature map P can be obtained as follows:

$$P = W_{\text{attention}} * X. \quad (4)$$

The feature map P is then downsampled by two strides to acquire pooling versions. In our experiments, the sample strides of two max-pooling operations in Fig. 2 are assigned to 4 and 2, respectively, and the feature maps (marked as $P1$ and $P2$) can be obtained. Finally, three maps including P, $P1$, and $P2$ are regarded as inputs of the decoder for subsequent operations.

C. Decoder

The decoder in the FR-CNN is employed to decode the features obtained from the encoder and the FRM and recover the resolution of the output radar reflectivity image. The architecture can be seen in Fig. 2. Similar to the encoder, the module consists of several CM modules including CM-2, CM-3, and CM-4, two transpose convolution operations, and three concatenation operations (marked as red circle C in the figure). The features P, $P1$, and $P2$ obtained from the FRM are regarded as inputs of the decoder. In the CM modules, the input is the concatenation of the previous module's result and the special output of the FRM. For example, the input of CM-3 is the concatenation of $P2$ and the output of CM-2. In this study, the kernel size of the convolution operations in CM-2, CM-3, and CM-4 is set to 3×3. The number of convolution kernels in the modules is assigned to 256, 128, and 64, respectively. After CM-4, the reconstructed CREF data corresponding to the input satellite observations can be obtained.

IV. Experiments and Results

In our experiments, the proposed FR-CNN is trained for 100 epochs to achieve the experimental results. Adam optimization [10] with initial learning rate 1×10^{-4} is adopted

TABLE I
PERFORMANCE COMPARISON OF DIFFERENT MODELS

Scheme	POD	FAR	CSI
baseline	0.586	0.432	0.427
U-Net	0.611	0.394	0.482
MVGG	0.621	0.362	0.511
FR-CNN	0.663	0.331	0.533

TABLE II
PERFORMANCE COMPARISON OF ABLATION EXPERIMENTS

Scheme	POD	FAR	CSI
baseline	0.586	0.432	0.427
baseline + SC (U-Net)	0.611	0.394	0.482
baseline + RB	0.644	0.346	0.524
baseline + RB + PAB	0.663	0.331	0.533

to optimize the regression object. An L1 loss function is employed to train the model as follows:

$$\min_{\omega} \frac{1}{N} \sum_{k=1}^{N} |f(x_k; \omega) - y_k| \tag{5}$$

where $f(x_k; \omega)$ is the retrieved CREF data of the kth input x_k, and y_k is the ground truth of the kth input. N is the number of training patches.

The contingency table approach is employed to evaluate the retrieval performance, as it is used commonly in atmospheric science areas [19]. Three widely used evaluation indices including the probability of detection (POD), false alarm ratio (FAR), and critical success index (CSI) with a threshold of 35 dBz [12] are utilized in this study.

Four experiments, baseline, U-Net, modified VGG (MVGG), and FR-CNN are conducted to demonstrate the performance of various models as follows.

1) *Baseline:* The architecture refers to the conventional encoder–decoder structure of the CNN, which is composed of an encoder and a decoder as shown in Fig. 2.
2) *U-Net:* The network is referred to [12], equipped with SC.
3) *MVGG:* The structure removes all pooling layers, the final convolution layer, and all fully connected layers of VGG-16 [11] and adds a convolution layer with the kernel number of 1 and size of 3×3.
4) *FR-CNN:* The proposed method in this letter.

A. Results and Analysis

For quantitative comparison, we calculate the values of POD, CSI, and FAR over the testing dataset, as shown in Table I. It is evident that the baseline network exhibits lower performance compared to other comparison methods. The baseline model achieves the lowest POD (0.586), CSI (0.427), and highest FAR (0.432), where the higher POD and CSI, the lower FAR correspond to better performance. This can be attributed to the lack of original information in the baseline network, which hinders its ability to accurately reconstruct CREF data. For U-Net, SC is used to preserve fine-scale information from shallower layers leading to better performance than the baseline network, that is, higher POD (0.611) and CSI (0.482) and lower FAR (0.394). MVGG is superior to U-Net, but it has comparatively worse performance than the FR-CNN, which can be attributed to the insufficient consideration of attention mechanisms. In contrast, the FR-CNN outperforms both U-Net and MVGG as it uses pristine information and attention mechanisms simultaneously.

Fig. 5 shows a case study of retrieved radar reflectivity using U-Net, MVGG, and FR-CNN. It is obvious that the

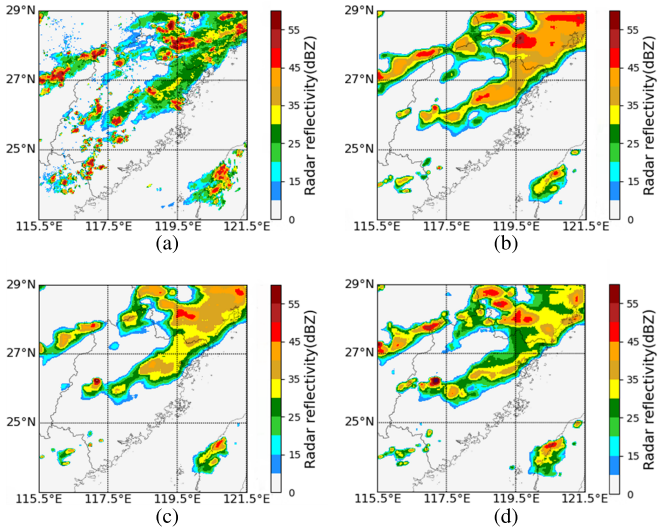

Fig. 5. Retrieved results at 08:30 UTC on 30 August 2019. (a) Radar observation. (b) U-Net. (c) MVGG. (d) FR-CNN.

FR-CNN can capture more detailed information than other models, showing the finer inner structure of convective cells, which indicates the effectiveness of the proposed method.

B. Ablation Experiments

In ablation experiments, the components including SC, RB, and PAB are incrementally added to the baseline, without other parameters and parts changed. The experimental results are shown in Table II, where it can be found that the progressive improvement in POD and CSI as the SC, RB, and PAB are successively incorporated into the baseline network, which confirms the effectiveness of the proposed PAB, FRM, and FR-CNN in enhancing the performance of radar reflectivity retrieval.

C. Generalization Performance Tests

To verify the generalization ability of the proposed method, U-Net and FR-CNN trained over the FJ area are directly used over the GZ area. POD, FAR, and CSI over the GZ area are regarded as quantity comparison indices. The FR-CNN has a higher POD value than U-Net (0.627 versus 0.582), a lower FAR value (0.351 versus 0.419), and a higher CSI (0.502 versus 0.448). The indices indicate that the proposed FR-CNN has better generalization performance than U-Net.

We further demonstrate a case study in the mountainous area where radar beams are often blocked resulting in the absence of radar echoes. The FR-CNN can reconstruct radar reflectivity images in those areas using satellite observations. Fig. 6 shows such a case over the GZ area. In the red rectangles, there are no radar echoes due to the blockage of radar beams, as is shown in Fig. 6(b). But from the satellite observation shown in Fig. 6(a),

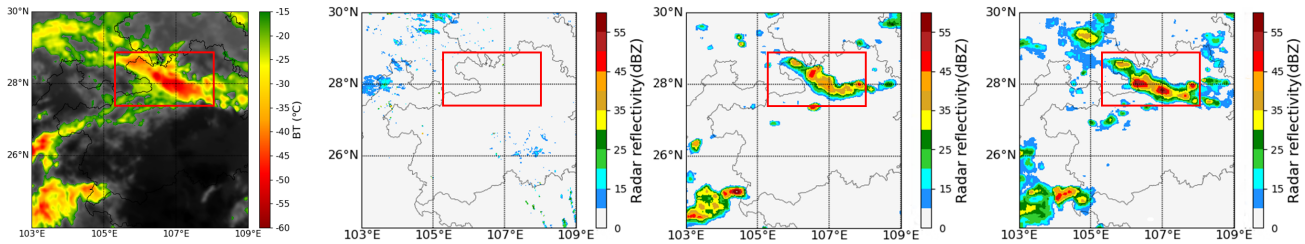

Fig. 6. Generalization example of U-Net and FR-CNN at 11:20 UTC on 30 May 2019. The regions without radar coverage in the GZ area are marked as red rectangles. (a) Satellite observation. (b) Radar observation. (c) U-Net. (d) FR-CNN.

a large storm can be clearly observed. U-Net and FR-CNN successfully reconstruct radar echoes in this area, whereas due to the usage of the FRM, the FR-CNN can provide the finer inner structure of storm cells than U-Net.

V. Conclusion and Future Works

This study proposes a novel CNN-based network called FR-CNN to reconstruct radar reflectivity data from geostationary satellite observations. Especially, an attention-based FRM is adopted in the FR-CNN. Compared with SC, the proposed module regards feature maps with more pristine information as inputs, which can effectively mitigate the problem of information scarcity during network propagation and capture more details of the inner structure of strong precipitation echoes. Experimental results demonstrate that the FR-CNN outperforms other methods such as U-Net. Case studies also show that the FR-CNN can reconstruct satisfactory CREF data over mountainous areas where radar echoes are absent due to beam blockage. In our future works, more machine-learning models such as XGBoost, GAN, and Transformer will be further explored to improve the retrieval ability of radar reflectivity reconstruction networks. Furthermore, as the BT is the top-down observational result and is often affected by the occlusion of clouds, the retrieved CREF cannot fully reflect lower-level features where there are strong echoes at high levels. This issue is worth a deeper study in the future.

Acknowledgment

The authors would like to thank NVIDIA Corporation for the donation of the graphics processing unit (GPU) used for this research. They also would like to thank the anonymous reviewers for providing careful reviews and comments on this letter.

References

[1] R. D. Roberts and S. Rutledge, "Nowcasting storm initiation and growth using GOES-8 and WSR-88D data," *Weather Forecasting*, vol. 18, no. 4, pp. 562–584, Aug. 2003.

[2] S. R. Proud, "Analysis of aircraft flights near convective weather over Europe," *Weather*, vol. 70, no. 10, pp. 292–296, Oct. 2015.

[3] J. Bech and M. Berenguer, "Predictability of heavy sub-hourly precipitation amounts for a weather radar based nowcasting system," in *Proc. EGU Gen. Assem. Conf. Abstr.*, 2015, p. 13945.

[4] L. Norin, "A quantitative analysis of the impact of wind turbines on operational Doppler weather radar data," *Atmos. Meas. Techn.*, vol. 8, no. 2, pp. 593–609, Feb. 2015.

[5] J. R. Mecikalski and K. M. Bedka, "Forecasting convective initiation by monitoring the evolution of moving cumulus in daytime GOES imagery," *Monthly Weather Rev.*, vol. 134, no. 1, pp. 49–78, Jan. 2006.

[6] J. R. Mecikalski, K. M. Bedka, S. J. Paech, and L. A. Litten, "A statistical evaluation of GOES cloud-top properties for nowcasting convective initiation," *Monthly Weather Rev.*, vol. 136, no. 12, pp. 4899–4914, Dec. 2008.

[7] J. R. Walker, W. M. MacKenzie, J. R. Mecikalski, and C. P. Jewett, "An enhanced geostationary satellite–based convective initiation algorithm for 0–2-h nowcasting with object tracking," *J. Appl. Meteorol. Climatol.*, vol. 51, no. 11, pp. 1931–1949, Nov. 2012.

[8] M. Duan et al., "Reconstruction of the radar reflectivity of convective storms based on deep learning and Himawari-8 observations," *Remote Sens.*, vol. 13, no. 16, p. 3330, Aug. 2021.

[9] J. Xia et al., "Machine learning-based weather support for the 2022 winter Olympics," *Adv. Atmos. Sci.*, vol. 37, no. 9, pp. 927–932, Sep. 2020.

[10] J. Si, B. Huang, H. Yang, W. Lin, and Z. Pan, "A no-reference stereoscopic image quality assessment network based on binocular interaction and fusion mechanisms," *IEEE Trans. Image Process.*, vol. 31, pp. 3066–3080, 2022.

[11] K. Simonyan and A. Zisserman, "Very deep convolutional networks for large-scale image recognition," in *Proc. 3rd Int. Conf. Learn. Represent. (ICLR)*, 2015, pp. 1–14.

[12] K. A. Hilburn, I. Ebert-Uphoff, and S. D. Miller, "Development and interpretation of a neural-network-based synthetic radar reflectivity estimator using GOES-R satellite observations," *J. Appl. Meteorol. Climatol.*, vol. 60, no. 1, pp. 3–21, Jan. 2021.

[13] F. Sun, B. Li, M. Min, and D. Qin, "Deep learning-based radar composite reflectivity factor estimations from Fengyun-4A geostationary satellite observations," *Remote Sens.*, vol. 13, no. 11, p. 2229, Jun. 2021.

[14] L. Yang et al., "Radar composite reflectivity reconstruction based on FY-4A using deep learning," *Sensors*, vol. 23, no. 1, p. 81, Dec. 2022.

[15] H. Raveendran and D. Thomas, "Image fusion using LEP filtering and bilinear interpolation," *Int. J. Eng. Trends Technol.*, vol. 12, no. 9, pp. 427–431, Jun. 2014.

[16] S. Woo, J. Park, J.-Y. Lee, and I. S. Kweon, "CBAM: Convolutional block attention module," in *Computer Vision—ECCV 2018*. Cham, Switzerland: Springer, 2018, pp. 3–19.

[17] K. He, X. Zhang, S. Ren, and J. Sun, "Deep residual learning for image recognition," in *Proc. IEEE Conf. Comput. Vis. Pattern Recognit. (CVPR)*, Jun. 2016, pp. 770–778.

[18] K. M. A. Hasan and S. Chakraborty, "GPU accelerated tensor computation of Hadamard product for machine learning applications," in *Proc. Int. Conf. Inf. Commun. Technol. Sustain. Develop. (ICICT4SD)*, Feb. 2021, pp. 1–5.

[19] R. J. Donaldson, R. M. Dyer, and M. J. Kraus, "An objective evaluator of techniques for predicting severe weather events," in *Proc. 9th Conf Severe Local Storms*. Boston, MA, USA: American Meteorological Society, 1975, pp. 321–326.